BNL-205665-2018-JAAM

Fe Stabilization by Intermetallic L10-FePt and Pt Catalysis En-hancement in L10-FePt/Pt Nanoparticles for Efficient Oxygen Reduc-tion Reaction in Fuel Cells

J. Li, D. Su

To be published in "Journal of The American Chemical Society"

February 2018

Center for Functional Nanomaterials

Brookhaven National Laboratory

U.S. Department of Energy

USDOE Office of Science (SC), Basic Energy Sciences (BES) (SC-22)

DISCLAIMER

Fe Stabilization by Intermetallic $L1_0$-FePt and Pt Catalysis Enhancement in $L1_0$-FePt/Pt Nanoparticles for Efficient Oxygen Reduction Reaction in Fuel Cells

Junrui Li,[†] Zheng Xi,[†] Yung-Tin Pan,[§] Jacob S. Spendelow,[§] Paul N. Duchesne,[//] Dong Su,[⊥] Qing Li,[⊤] Chao Yu,[†] Zhouyang Yin,[†] Bo Shen,[†] Yu Seung Kim,[§] Peng Zhang,[//] and Shouheng Sun[*,†]

[†]Department of Chemistry, Brown University, Providence, Rhode Island 02912, United States

[§]Materials Physics and Application Division, Los Alamos National Laboratory, Los Alamos, New Mexico, 87545, United States

[//]Department of Chemistry, Dalhousie University, Halifax, Nova Scotia B3H 4R2, Canada

[⊥]Center for Functional Nanomaterials, Brookhaven National Laboratory, Upton, New York 11973, United States

[⊤]School of Materials Science and Engineering, Huazhong University of Science and Technology, Wuhan, Hubei 430074, People's Republic of China

ABSTRACT: We report in this article a detailed study on how to stabilize a first-row transition metal (M) in an intermetallic $L1_0$-MPt alloy nanoparticle (NP) structure and how to surround the $L1_0$-MPt with an atomic layer of Pt to enhance the electrocatalysis of Pt for oxygen reduction reaction (ORR) in fuel cell operation conditions. Using 8 nm FePt NPs as an example, we demonstrate that Fe can be stabilized more efficiently in a core/shell structured $L1_0$-FePt/Pt with a 5 Å Pt shell. The presence of Fe in the alloy core induces the desired compression of the thin Pt shell, especially the 2 atomic layers of Pt shell, further improving the ORR catalysis. This leads to much enhanced Pt catalysis for ORR in 0.1 M $HClO_4$ solution (both at room temperature and 60°C) and in the membrane electrode assembly (MEA) at 80°C. The $L1_0$-FePt/Pt catalyst has a mass activity of 0.7 A/mg_{Pt} from the half-cell ORR test and shows no obvious mass activity loss after 30,000 potential cycles between 0.6 V and 0.95 V at 80°C in the MEA, meeting the DOE 2020 target (<40% loss in mass activity). We are extending the concept and preparing other $L1_0$-MPt/Pt NPs, such as $L1_0$-CoPt/Pt NPs, with reduced NP size as a highly efficient ORR catalyst for automotive fuel cell applications.

INTRODUCTION

A proton exchange membrane fuel cell (PEMFC) converts chemical energy stored in fuel (such as hydrogen or alcohol) into electricity via the coupled oxidation of the fuel and reduction of oxygen.[1] In this energy conversion device, platinum (Pt) is an essential component as both the oxidation and the reduction catalysts. However, this use of Pt is not without limit. Without weighing the Pt abundance issue, the Pt catalyst itself shows undesirably sluggish 4-electron oxygen reduction reaction (ORR) kinetics and lacks the desired long-term stability in the corrosive reaction environment. As a result, extensive research efforts have been devoted to improving ORR catalysis on Pt by understanding the binding energies of Pt with numerous oxygen-containing reaction intermediates and by alloying Pt with a first-row transition metal, M.[2,3] Despite the impressive initial activity demonstrated, these MPt alloys are often prepared in a solid solution A1 structure and the alloyed M is difficult to be stabilized by this A1 structure in the corrosive ORR condition, especially at elevated temperatures more relevant to the PEMFC operation, resulting in extensive M loss and compromising all benefits the M brings to the Pt catalysis.[2]

An imperative question to answer is if an improved MPt nanocatalyst can be developed to exhibit higher activity and durability in the PEMFC operating conditions. Among all methods demonstrated to stabilize M in the MPt alloy structure for the ORR catalysis, intermetallic MPt structure, especially the tetragonal $L1_0$-MPt, attracts much attention.[4,5] Compared with the solid solution A1 structure in which M and Pt occupy randomly the face centered cubic (fcc) lattice, the $L1_0$-MPt structure has M(3d)-Pt(5d) strongly coupled along the crystallographic *c*-direction, stabilizing M against oxidation and etching in an acidic ORR condition at room temperature,[4,5] though leaching can still occur at elevated temperatures. Herein, using FePt as an example, we demonstrate a modified approach to 8 nm core/shell $L1_0$-FePt/Pt nanoparticles (NPs) with $L1_0$-FePt core and an atomically thin (5 Å) Pt shell. In this core/shell structure, Fe is better stabilized and Pt shell shows more efficient ORR catalysis than the 8 nm Pt NPs not only at room temperature or 60°C in 0.1 M $HClO_4$ solution, but also at 80°C in the membrane electrode assembly (MEA) test condition.

EXPERIMENTAL SECTION

Chemicals and Materials: All chemicals were used without further purifications. $Mg(acac)_2$ (anhydrous, 98%) (acac = aceylacetonate) and $Pt(acac)_2$ (98%) were purchased from Strem Chemicals. Oleylamine (70%), oleic acid (90%), 1-octadecene (90%), benzyl ether (98%), $Fe(CO)_5$, 1,2-dodecanediol (90%) and Nafion (5% in a mixture of 2-

propanol and water) were purchased from Sigma-Aldrich. The commercial Pt catalyst (product code: 591278, 20% mass loading on carbon, Pt particle diameter at 2.0-3.0 nm) was purchased from Fuel Cell Store. Commercial TKK TEC10E20E Pt catalyst (mass loading of 20 %) was obtained from Tanaka.

Synthesis of dumbbell-like FePt-Fe_3O_4 NPs. This synthesis was modified from what was published.[5] 0.2 g $Pt(acac)_2$, 1.4 mL oleylamine and 1.3 mL oleic acid were dissolved in 10 mL 1-octadecene in a four-neck reaction flask. The mixture was stirred and degassed at 120°C under a gentle nitrogen flow for 30 min. Under a blanket of nitrogen, $Fe(CO)_5$ (0.05 mL) was injected into the mixture. The reaction solution was then heated to 220°C at a rate of 5°C/min and kept at this temperature for 30 min. The solution was further heated to 300°C at a rate of 10°C/min and maintained at 300°C for 10 min before it was cooled to room temperature. After being precipitated and washed twice with 2-propanol, the product, dumbbell-like FePt-Fe_3O_4 NPs (**Figure S1A**), was collected by centrifugation (8500 rpm, 8 min) and dispersed in hexane for further use.

Synthesis of MgO-coated FePt-Fe_3O_4 NPs. This synthesis was modified from what was published.[5] 0.4 g $Mg(acac)_2$, 0.37 g 1,2-dodecanediol, 0.9 mL oleylamine, 0.6 mL oleic acid were dissolved in 18 mL benzyl ether under stirring and degassed at 120°C in a four-neck reaction flask. 40 mg FePt-Fe_3O_4 NPs were added into the mixture. The reaction solution was heated to 300°C at a rate of 8°C/min and kept at this temperature for 1 h before it was cooled to room temperature. The product, MgO-coated FePt-Fe_3O_4 NPs (**Figure S1B**) was precipitated and washed twice with ethanol, centrifuged (8500 rpm, 8 min) and redispersed in hexane.

Preparation of carbon-supported core/shell $L1_0$-FePt/Pt. Ketjen-300J carbon (C) was suspended in hexane under sonication for 20 min, then the MgO-coated FePt-Fe_3O_4 NPs were added dropwise into the suspension (C/NP mass ratio = 1:1). After 1 h sonication, the C-supported MgO-coated NPs were dried and annealed under 95% Ar + 5% H_2 at 700°C for 6 h to obtain C-MgO-$L1_0$-FePt. MgO coating was then removed by acid etching for 20 min in 0.1 M $HClO_4$. The C-$L1_0$-FePt NPs were then stirred in 0.1 M $HClO_4$ at 60°C in air for 12 h, followed by annealing under 95% Ar + 5% H_2 at 400°C for 2 h, which gave C-$L1_0$-FePt/Pt NPs for further study.

Synthesis of A1-FePt NPs and their conversion to 8 nm Pt catalysts. The A1-FePt NPs were prepared in the same manner as the dumbbell- FePt-Fe_3O_4 but without the 300°C heating condition. The solution of 0.2 g $Pt(acac)_2$, 1.4 mL oleylamine and 1.3 mL oleic acid and 10 mL 1-octadecene was degassed at 120°C under a gentle nitrogen flow for 30 min. Under a blanket of nitrogen, $Fe(CO)_5$ (0.16 mL) was injected into the solution. The solution was heated to 220°C at a rate of 3°C/min and kept at this temperature for 1 h before it was cooled to room temperature. After being precipitated and washed twice with 2-propanol and collected by centrifugation (8500 rpm, 8 min), 8 nm A1-$Fe_{43}Pt_{57}$ NPs were obtained and then deposited on the Ketjen-300J carbon support (C/NP mass ratio = 1:1), as described in the preparation of C-$L1_0$-FePt/Pt. The C-A1-FePt was stirred in 0.1 M $HClO_4$ at 60°C in air overnight to reach a final composition of ($Fe_{15}Pt_{85}$). The acid treated sample was washed with water twice, dried in air and annealed at 400°C for 2 h under 95% Ar + 5% H_2. The product, was denoted as C-Pt with Pt being 8 nm NPs, and used as a control.

Characterization. Bruker AXS D8-Advanced diffractometer with Cu Kα radiation (λ = 1.5418 Å) was used to collect X-ray diffraction (XRD) patterns of the C-NPs. Transmission electron microscopy (TEM) images were obtained on a Philips CM20 operating at 200 kV. A Hitachi HD2700C (200 kV) was used for scanning transmission electron microscopy (STEM) and high-angle annular dark-field (HAADF) imaging analyses with a probe aberration corrector at the Center for Functional Nanomaterials, Brookhaven National Lab. The electron energy loss spectroscopy (EELS) line-scan was obtained by a high-resolution Gatan-Enfina ER with a probe size of 1.3 Å. A power law function was used for EELS background subtraction. Magnetic hysteresis loop was measured on a Quantum Design Superconducting Quantum Interface Device (SQUID) with a field up to 70 KOe. The inductively coupled plasma-atomic emission spectroscopy (ICP-AES) results were obtained on a JY2000 Ultrace ICP atomic emission spectrometer equipped with a JY AS 421 autosampler and 2400g/mm holographic grating. X-ray absorption spectroscopy (XAS) measurements were performed using the Sector 20-BM beamline of the Advanced Photon Source at Argonne National Laboratory. Sample powders were packed between Kapton windows, and cooled to 90 K in a Displex cryostatic sample holder during the measurements to enhance the EXAFS signal intensity via suppression of thermal lattice vibrations. The end-station was equipped with a double-crystal Si (111) monochromator for wavelength selection, which was detuned to 80% in order to help reject higher harmonics of the desired energy; a toroidal focusing mirror was also employed to further enhance harmonic rejection. Gas-ionization detectors were used to measure the absorption spectra of the W L_3- edge and a 12-element Ge fluorescence detector was used to collect spectra of the Pd K-edge. Data processing and EXAFS fitting were performed using WinXAS software[6] in conjunction with scattering path amplitude and phase functions calculated using the computer codeFEFF8.2. [7]

Catalyst ink preparation and electrochemical measurements: Catalyst ink for electrochemical study was prepared by mixing 2 mg C-NPs with 800 µL ultrapure water, 200 µL 2-propanol and 10 µL Nafion solution (5 wt%) for 1 h. 20 µL of catalyst ink was then deposited onto the glassy carbon rotating disk electrode (5 mm in diameter) for electrochemical measurements. An Autolab 302 potentiostat together with Ag/AgCl (4 M KCl) as a reference electrode, and graphite bar as a counter electrode was used to obtain cyclic voltammetry (CV) and linear scanning voltammetry (LSV) curves. The $L1_0$-FePt/Pt catalyst was first subject to CV scanning between 0.05 and 1.3 V at 100 mV/s in N_2-saturated 0.1 M $HClO_4$ until a stable CV curve was obtained (typically 200 cycles). ORR polarization curves were recorded by LSV technique at a scan rate of 20 mV/s in O_2-saturated 0.1 M $HClO_4$ with GC-RDE rotating at 1600 rpm. Accelerated durability tests (ADT) of the catalysts for ORR were conducted by cycling the potential between 0.6 and 1.0 V at 100 mV/s at 60°C and room temperature, respectively. To investigate the influence of temperature on the ORR activity of the catalysts, the LSV tests were conducted on the $L1_0$-FePt/Pt NPs at room temperature, 40 °C and 60 °C, respectively.

MEA Preparation and Fuel Cell Testing. Catalysts were incorporated into MEAs through a decal transfer process: cata-

lysts were mixed with tetrabutylammonium (TBA)-form ionomer and dispersed in a glycerol-based ink, followed by painting the ink onto 5 cm^2 decals. Catalyst layer was transferred from decal to Na^+-form membrane by hot-pressing. Prior to measurement in fuel cell, MEA was protonated in boiling 0.5 M H_2SO_4, and MEA break-in was conducted by holding at 0.6 V overnight and performing voltage steps. H_2-air fuel cell testing was carried out in a single cell using a commercial fuel cell test system (Fuel Cell Technologies Inc.). The MEA was sandwiched between two graphite plates with single-serpentine flow channels machined in them. The cell was operated at 80°C, with 150 kPa_{abs} H_2/air or H_2/O_2, 100 % relative humidity, and a gas flow rate of 100-200 sccm. Catalyst mass activity was measured by holding the potential at 0.9 V iR-free for 5 min, with the current averaged during the last 1 min.. The electrochemical active surface area (ECASA) was obtained by calculating HUPD charge in CV curves between 0.1-0.4 V (0.45-0.55 V background subtracted); assuming a value 210 μC/cm^2 for the adsorption of a hydrogen monolayer on Pt. (CV curves were obtained under 150 kPa_{abs} H_2/N_2, 30 °C, >100% RH, 100-200 sccm) The potential cycling accelerated stress test (AST) was conducted by using trapezoidal wave method from 0.6 V to 0.95 V with 0.5 s rise time and 2.5 s hold time.

RESULTS AND DISCUSSION

Material synthesis and characterization. Monodisperse 8 nm core/shell FePt/Pt NPs with $L1_0$-FePt core and atomically thin Pt were synthesized via a method modified from the previous report.[5] Briefly, dumbbell-like FePt-Fe_3O_4 NPs (shown in **Figure S1A**) were first obtained by co-reduction of iron pentacarbonyl ($Fe(CO)_5$ and platinum acetylacetonate ($Pt(acac)_2$) at 300°C. These dumbbell NPs were coated with MgO (**Figure S1B**) and then supported onto Ketjen-black EC-300J carbon (C), followed by annealing treatment under 95% Ar + 5% H_2 at 700°C for 6 h to reduce Fe_3O_4 to Fe and to allow Fe/Pt inter-diffusion into $L1_0$-structure. MgO was removed by immersing the annealed C-NPs in 0.1 M $HClO_4$ at room temperature to obtain C-$L1_0$-FePt NPs. Surface layers of Fe were removed by immersing the $L1_0$-FePt NPs in the warm (60°C) 0.1 M $HClO_4$ solution for 12 h, converting the NPs to the core/shell FePt/Pt with defective Pt layers, $L1_0$-FePt/Pt_d. The defective Pt layer was smoothened by further annealing treatment under 95% Ar + 5% H_2 at 400°C for 2 h, giving the core/shell structured catalyst, $L1_0$-FePt/Pt.

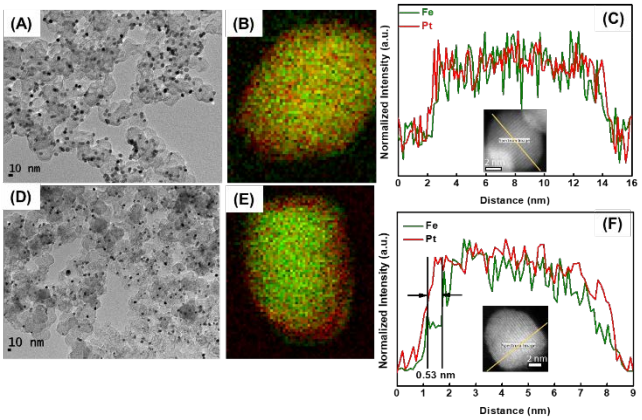

Figure 1. (**A**) TEM image of C-$L1_0$-FePt NPs. (**B**) 2D EELS elemental mapping image of $L1_0$-FePt NPs, where Fe is colored green and Pt is colored red. (**C**) STEM-EELS line scan of a $L1_0$-FePt NP. (**D**) TEM image of C-L10-FePt/Pt NPs. (**E**) 2D EELS elemental mapping image a $L1_0$-FePt/Pt NP, where Fe is colored green and Pt is colored red. (**F**) STEM-EELS line scan of a $L1_0$-FePt/Pt NP.

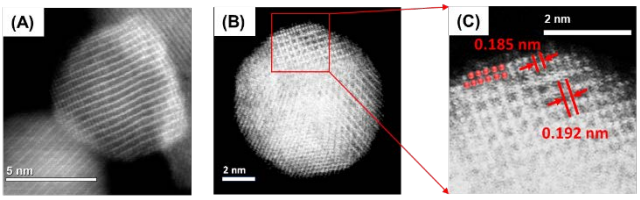

Figure 2. (**A**) HAADF-STEM image of a representative $L1_0$-FePt NP. (**B**) HAADF-STEM image of a representative $L1_0$-FePt/Pt NP with about 2 atomic layers of Pt shell and its enlarged image (**C**).

As shown in the TEM image (**Figure 1A**), the $L1_0$-FePt NPs are well dispersed on the C support and have an average size of 8.0 nm ± 0.5 nm. The electron energy loss spectroscopy (EELS) elemental mapping (**Figure 1B**) and line scan crossing a single NP (**Figure 1C and inset**) show that Fe and Pt are uniformly distributed within the NP. The same analyses of the $L1_0$-FePt/Pt (**Figure 1D, E, F and inset**) show that it has a core/shell structure with an intermetallic $L1_0$-FePt core and a thin (0.53 nm, ~2 atomic layers) Pt layer. High-angle annular dark-field scanning transmission electron microscopy (HAADF-STEM) image (**Figure 2A**) shows that the $L1_0$-FePt NP has the characteristic alternating Fe and Pt atom stacking in one direction. The $L1_0$-FePt/Pt core/shell is further confirmed by a representative HAADF-STEM image (**Figure 2B and C**) (the atomically thin Pt shell is highlighted with red dots). The lattice fringe of the $L1_0$-FePt core is 0.192 nm (**Figure 2C**) which corresponds to the $L1_0$-FePt (110) (0.193 nm, JCPDS 65-1051). The atomic Pt-layer has an average lattice fringe spacing of 0.185 nm, which is smaller than the common Pt (200) interplanar distance (0.196 nm, JCPDS 4-0802), indicating that the Pt lattice in this thin layer is compressed due to its epitaxial link with $L1_0$-FePt. Inductively coupled plasma atomic emission spectroscopy (ICP-AES) analysis was used to measure the Fe/Pt composition change of A1-FePt, $L1_0$-FePt and $L1_0$-FePt/Pt immersed in 0.1 M $HClO_4$ at 60°C in air (**Figure S3**). Starting at Fe/Pt = 51%/49%, the A1-FePt lost Fe quickly after 2 h of immersion into the acid, the Fe content was reduced to 20% and further dropped to below 15% after 24 h exposure in acid. As a comparison, the $L1_0$-FePt NPs showed much better stability—its Fe content was at 43% after 12 h of etching. Once annealed at 400°C to form $L1_0$-FePt/Pt, its Fe content was stabilized at 42~43% in the 24 h etching period. From this etching experiment, we can see that the $L1_0$-FePt structure is much more effective in

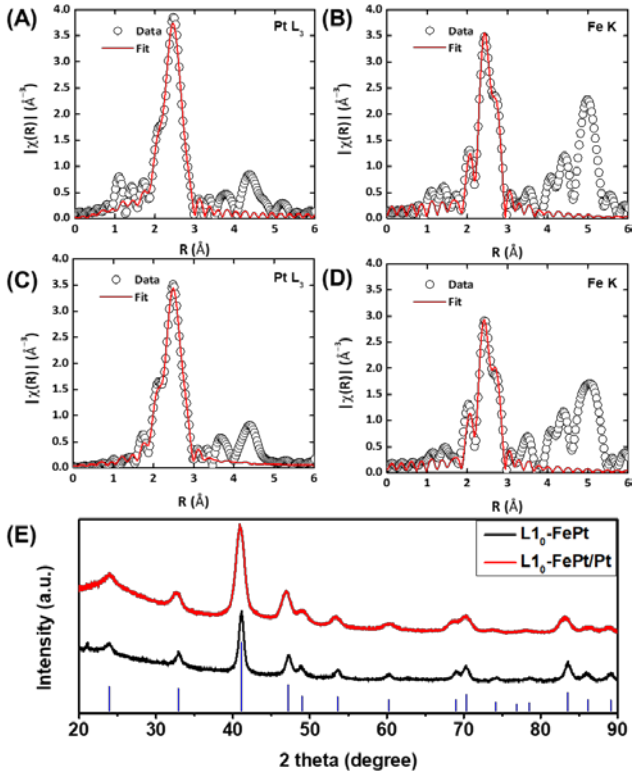

Figure 3. (**A-D**) EXAFS spectra of Pt L_3 edge (**A**) and Fe K edge (**B**) of the $L1_0$-FePt NPs, as well as Pt L_3 edge (**C**) and Fe K edge (**D**) of the $L1_0$-FePt/Pt NPs. (**E**) XRD patterns of the $L1_0$-FePt and $L1_0$-FePt/Pt. The standard peaks of $L1_0$ (fct-type) FePt are shown in blue lines (JCPDS: 65-1051).

stabilizing Fe from deep etching in the warm (60°C) 0.1 M $HClO_4$ solution.

Structural analysis of the $L1_0$-FePt/Pt NPs. X-rayabsorption near edge structure (XANES) and extended X-rayabsorption fine structure (EXAFS) were used to analyze the structure features of the core/shell NPs. In **Figure S4**, the "white line" peaks of both FePt NP samples are more intense than the Pt foil reference, indicating that d-electron density on Pt in the NP samples is reduced, consistent with the result reported on Pt-based NPs.[8] Pt L3-edge and Fe K-edge spectra (both experimental (black) and fitted (red)) are shown in **Figure 3A-D** and the related parameters are listed in **Table S1**. We can see that in the $L1_0$-FePt NPs, the Fe-Pt coordination number (CN) is at 6, but the Fe–Fe CN is small, only about 2.5, suggesting that in this kind of NP structure, the Fe-Fe bonding is localized only in a limited dimension (2-dimension in the $L1_0$ structure), but the Fe-Pt bonding is in 3-dimension. The Pt–Pt bond length (2.713 Å) is significantly shorter than the bulk Pt value (2.775 Å) due to the incorporation of smaller Fe atoms into the alloy structure. The same alloy effect leads to the observed Fe–Fe bond length increase from the bulk value of 2.482 Å to the NP value of 2.69 Å. In the core/shell $L1_0$-FePt/Pt structure, the total Fe CN (CN_{Fe-Fe} + CN_{Fe+Pt}) is increased from 6 to 7, providing additional evidence that Fe is absent from the surface.[9] The formation of a smooth Pt layer in the $L1_0$-FePt/Pt can be further characterized by its CO stripping behavior.[10] As shown in **Figure S5**, the sharper CO oxidation peak from the $L1_0$-FePt/Pt shifts to a more positive potential than that (broader) from the $L1_0$-FePt/Pt_d, indicating

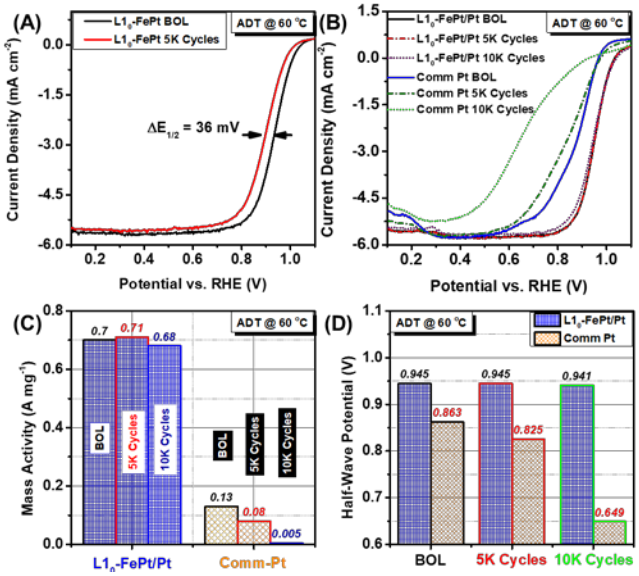

Figure 4. (**A**) ORR polarization curves of the $L1_0$-FePt tested at beginning of life (BOL) and after ADT test (5,000 cycles at 60°C in oxygen-saturated 0.1 M $HClO_4$). (**B**) ORR polarization curves of the $L1_0$-FePt/Pt and commercial Pt tested at BOL and after ADT test (5,000 cycles and 10,000 cycles at 60°C in oxygen-saturated 0.1 M $HClO_4$). Mass activity (**C**) and half-wave potential (**D**) changes of the $L1_0$-FePt/Pt and the commercial Pt catalysts.

that after annealing treatment, a smooth Pt-layer is indeed formed on the $L1_0$-FePt/Pt surface. Compared to the $L1_0$-FePt/Pt_d, the presence of the smooth Pt layer in the $L1_0$-FePt/Pt shifts the Pt-O reduction potential positively (**Figure S6**), indicating that the O binding is weakened on the smooth Pt surface, which should promote ORR catalysis.[11] X-ray power diffraction (XRD) patterns of both $L1_0$-FePt and $L1_0$-FePt/Pt show the typical $L1_0$ structure (**Figure 3E**), but the $L1_0$-FePt/Pt has a slightly broader peak, indicating that the removal of surface Fe also reduces the crystal domain sizes of the $L1_0$-structure. Despite this change, the $L1_0$-FePt/Pt NPs still show high room temperature coercivity at 33.8 kOe (**Figure S7**), indicating a high degree (>80%) of Fe/Pt ordering in the $L1_0$-FePt core structure.[12]

Electrochemical study and fuel cell test. To study the NP catalysis for the ORR, the C-NP-covered electrode was subject to 200 cycles of potential scans between 0 and 1.2 V (vs RHE) in the N_2-saturated 0.1 M $HClO_4$ to condition the catalyst till a stable CV curve was obtained. OR polarization curves were first obtained at room temperature so that this set of data could be used to compare with the reported ones. The ORR kinetics are quite temperature dependent as shown **Figure S8A**, which is consistent with what has been observed that higher temperature provides faster ORR kinetics and better ORR activity.[13] Accelerated durability test (ADT) was conducted at 60°C to demonstrate the catalyst stability at this temperature. Although the $L1_0$-FePt shows the stable ORR performance with a half-wave potential of 0.945 V at room temperature without obvious activity loss after 5,000 cycles (**Figure S8B**), it suffers an obvious activity loss at 60°C with the half-wave potential negatively shifting of 36 mV (**Figure 4A**) due very likely to the formation of the defective Pt surface ($L1_0$-FePt/Pt_d) in acid after the ADT test. Higher temperature (60°C) increases atom mobility and may result in more severe Fe loss and the re-formation

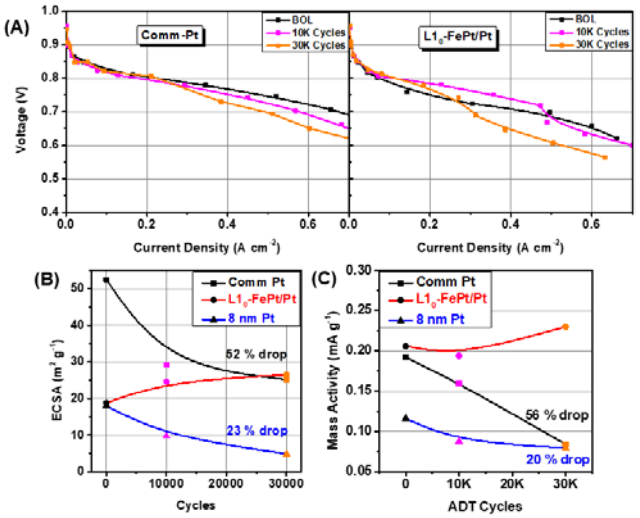

Figure 5. (**A**) H_2-air fuel cell polarization curves recorded on MEAs assembled with commercial TKK-Pt and $L1_0$-FePt/Pt catalysts, respectively. (**B**) ECASA and (**C**) mass activity of the commercial TKK-Pt, $L1_0$-FePt/Pt and 8 nm Pt catalysts during ADT up to 30,000 cycles in the fuel cell.

of defective Pt surface. In contrast, the $L1_0$-FePt/Pt with smooth Pt layer shows excellent stability at 60°C without obvious ORR performance loss after 10,000 cycles (**Figure 4B**). In the same 60°C test condition, the commercial C-Pt (Fuel Cell Store, 2.0-3.0 nm Pt with 20% mass loading) shows a significant drop in both mass activity @ 0.9 V from 0.13 A mg^{-1} to 0.005 A mg^{-1} (**Figure 4C**) and half-wave potential (from 0.863 V to 0.649 V) (**Figure 4D**). As a comparison, the mass activity of the $L1_0$-FePt/Pt drops only from 0.70 A mg^{-1} to 0.68 A mg^{-1} @0.9 V (**Figure 4C**) and its ORR half-wave potential shifts from 0.945 V to 0.941 V (**Figure 4D**). TEM analyses indicate that the drop of the ORR performance of the C-Pt is obviously caused by the NP aggregation in the 60°C ADT test condition (**Figure S9A, B**), which leads to drastic decrease in its electrochemically active surface area (ECASA) (**Figure S9C**). In contrast, the morphologies shown in TEM images and ECASA of the $L1_0$-FePt/Pt are nearly unchanged in the same test condition (**Figure S10**).

A good ORR catalyst must meet the 2020 DOE target (0.44 A mg^{-1} in mass activity) in a fuel cell device[2a,3a] with acceptable durability (< 40% loss in mass activity)[14]. In some previously studied intermetallic FePt work, carbon coatings were added to protect the FePt NPs to show promising fuel cell performance, but the key ADT performance and mass activity data were not reported.[15] We studied the fuel cell performance of our $L1_0$-FePt/Pt by using the DOE-Fuel Cell Tech Team (DOE/FCTT) protocol. We prepared MEAs with cathodes containing either $L1_0$-FePt/Pt or commercial TKK TEC10E20E C-Pt (~2 nm). The MEAs were activated by holding at 0.6 V overnight and performing voltage steps. ADT was conducted by following the DOE/FCTT protocol: a trapezoidal wave potential cycle between 0.6 V and 0.95 V in N_2 at 80°C. The mass activity and ECASA was calculated based on the measured current and Pt loading of the commercial TKK Pt (0.122 mg_{Pt} cm^{-2}) and $L1_0$-FePt/Pt (0.113 mg_{Pt} cm^{-2}). H_2/air polarization curves in **Figure 5A** show that the performance of the TKK catalyst constantly drops, having a 52% loss in initial ECASA (**Figure 5B**) and a 56% loss in mass activity at 0.9 V (**Figure 5C**) after 30,000 cycles. In contrast, the related ECASA and mass activity of the $L1_0$-

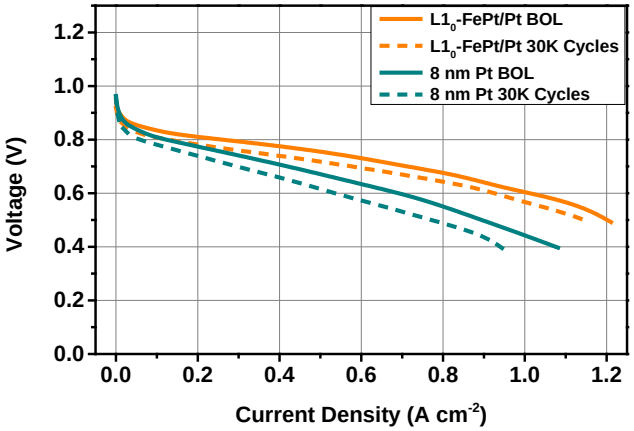

Figure 6. H_2-air fuel cell polarization curves recorded from the MEAs assembled with the $L1_0$-FePt/Pt (22 wt% of Pt loading ratio, Pt loading of 0.103 mg_{Pt}/cm^2), and 8 nm Pt catalysts (23 wt% of Pt loading ratio, Pt loading of 0.097 mg_{Pt}/cm^2) respectively.

FePt/Pt are much more stable with no drop during the ADT test, meeting the DOE 2020 target on catalytic activity loss (< 40% loss in mass activity). The initial and EOL (end-of- life) mass activity values of $L1_0$- FePt/Pt are 0.21 and 0.23mA g^{-1}, respectively, which are much higher than those of the commercial TKK Pt. However,its mass activity in fuel cell is still below the DOE 2020 target (0.44 A mg^{-1}) due likely to the larger NP size (8 nm FePt/Pt vs ~2 nm TKK Pt). We are working to prepare new $L1_0$-MPt/Pt NPs with sizes smaller than 5 nm to improve the mass activity.

To further support our argument that the enhanced catalysis of the $L1_0$-FePt/Pt arises from the compressed Pt layer coated over the intermetallic NP core, not from the larger size (8 nm NPs vs the commercial TKK 2 nm Pt NPs), we prepared C-Pt with Pt NPs in 8 nm (**Figure S11**). We studied the ORR catalysis of this C-Pt and observed the apparent drop in both activity and ECASA after 5,000 ADT cycles at 60°C (**Figure S12, Figure 4B&C**). Its initial mass activity is only at 0.11 mA gPt^{-1}, lower than the value of the commercial TKK Pt (0.19 mA gPt^{-1}). The 8 nm Pt may have better stability (20% drop in mass activity and 23% loss in ECASA) compared to the commercial TKK Pt during the ADT test, but after 30,000 ADT cycles, the 8 nm Pt and the commercial TKK Pt have similar mass activity of ~0.08 mA g_{Pt}^{-1}, much lower than that of the $L1_0$-FePt/Pt (0.23 mA g_{Pt}^{-1}). **Figure 6** compares the polarization curves of the $L1_0$-FePt/Pt and 8 nm Pt tested at BOL (beginning-of-life) and 30,000 cycles, respectively. The $L1_0$-FePt/Pt shows BOL and EOL performance superior to the 8 nm Pt in the whole potential range, demonstrating that it is the intermetallic $L1_0$-FePt structure, not the 8 nm size, that gives the excellent activity and durability of the core/shell NPs in the fuel cell test.

CONCLUSIONS

In this paper, we provide some concrete evidences that intermetallic core/shell $L1_0$-FePt/Pt with ~2 atomic layers of Pt shell is chemically stable against fast/deep Fe etching for active ORR catalysis. The smooth thin Pt shell is compressed due to its epitaxial binding with the $L1_0$-FePt core and the core/shell $L1_0$-FePt/Pt NPs become catalytically more active than either the 8 nm Pt NPs or the commercial TKK-Pt (2 nm) NPs, showing superior mass activity (0.7 A mg^{-1} at 0.9 V) and much better durability under the fuel cell testing (without no-

ticeable activity loss in the 30,000 fuel cell testing cycles between 0.6 V and 0.95 V at 80°C). As a comparison, the commercial TKK-Pt lost 56 % of its mass activity in the same fuel cell testing condition. We are working to reduce the size of the $L1_0$-FePt NPs to achieve higher mass activity. Moreover, we are extending the concept and are preparing other $L1_0$-MPt/Pt (M = Co, or CoNi) NPs as a robust catalyst for PEMFC applications.

ASSOCIATED CONTENT

Supporting Information. Figure S1~Figure S12, and Table S1 are included in the supplementary document.

AUTHOR INFORMATION

Corresponding Author

* ssun@brown.edu.

Notes

The authors declare no conflicts of interests.

ACKNOWLEDGMENT

The work was supported by US Department of Energy, Energy Efficiency and Renewable Energy, Fuel Cell Technology Office. Los Alamos National Laboratory is operated by Los Alamos National Security, LLC under Contract DE-AC52-06NA25396. This research used resources of the Advanced Photon Source, an Office of Science User Facility operated for the U.S. Department of Energy (DOE) Office of Science by Argonne National Laboratory, and was supported by the U.S. DOE under Contract No. DE-AC02-06CH11357, and the Canadian Light Source and its funding partners. Part of electron microscopy work was carried out at the Center for Functional Nanomaterials, Brookhaven National Laboratory (BNL), which is supported by the DOE, Office of Basic Energy Sciences, under contract DE-SC-0012704. Q. L. thanks for financial support from National Nature Science Foundation of China (21603078) and National Materials Genome Project (2016YFB0700600).

REFERENCES

1 R. Borup, J. Meyers, B. Pivovar, Y. S. Kim, R. Mukundan, N. Garland, D. Myers, M. Wilson, F. Garzon, D. Wood. *Chem. Rev*. **2007**, 107, 3904-3951.

2 (a) I. E. L. Stephens, J. Rossmeisl, I. Chorkendorff. *Science* **2016**, 354, 1378-1379. (b) V. R. Stamenkovic, B. S. Mun, M. Arenz, K. J. Mayrhofer, C. A. Lucas, G. Wang, P. N. Ross, N. M. Markovic. *Nat. Mater.* **2007**, 6, 241-247. (c) P. Strasser, S. Koh, T. Anniyev, J. Greeley, K. More, C. Yu, Z. Liu, S. Kaya, D. Nordlund, H. Ogasawara, M. F. Toney, A. Nilsson, *Nat. Chem.* **2010**, 2, 454-460.

3 (a) C. Chen, Y. Kang, Z. Huo, Z. Zhu, W. Huang, H. L. Xin, J. D. Snyder, D. Li, J. A. Herron, M. Mavrikakis, M. Chi, K. L. More, Y. Li, N. M. Markovic, G. A. Somorjai, P. Yang, V. R. Stamenkovic. *Science* **2014**, 343, 1339-1343. (b) X. Huang, Z. Zhao, L. Cao, Y. Chen, E. Zhu, Z. Lin, M. Li, A. Yan, A. Zettl, Y. M. Wang, X. Duan, T. Mueller, Y. Huang. *Science* **2015**, 348, 1230-1234. (c) M. Li, Z. Zhao, T. Cheng, A. Fortunelli, C. Y. Chen, R. Yu, Q. Zhang, L. Gu, B. V. Merinov, Z. Lin. *Science* **2016**, 354, 1414-1419.

4 (a) G. Jiang, H. Zhu, X. Zhang, B. Shen, L. Wu, S. Zhang, G. Lu, Z. Wu, S. Sun, *ACS Nano* **2015**, 9, 11014-11022. (b) D. Wang, H. L. Xin, R. Hovden, H. Wang, Y. Yu, D. A. Muller, F. J. DiSalvo, H. D. Abruña. *Nat. Mater.* **2013**, 12, 81-87. (c) S. Zhang, S. Guo, H. Zhu, D. Su, S. Sun. *J. Am. Chem. Soc.* **2012**, 134, 5060-5063.

5 Q. Li, L. Wu, G. Wu, D. Su, H. Lv, S. Zhang, W. Zhu, A. Casimir, H. Zhu, A. Mendoza-Garcia, S. Sun, *Nano Lett.* **2015**, 15, 2468-2473.

6 T. Ressler. *J. Synchrotron Radiat.* **1998**, 5, 118-122.

7 A. Ankudinov, B. Ravel, J. Rehr, S. Conradson. *Phys. Rev. B.* **1998**, 58, 7565-7576.

8 P. Duchesne, G. Chen, N. Zheng, P. Zhang. *J. Phys. Chem. C.* **2013**, 117, 26324−26333.

9 J. Durst, M. Lopez-Haro, L. Dubau, M. Chatenet, Y. Soldo-Olivier, L. Guétaz, P. Bayle-Guillemaud, F. Maillard. *J. Phys. Chem. Lett*. **2014**, 5, 434-493.

10 (a) N. P. Lebedeva, A. Rodes, J. M. Feliu, M. T. M. Koper, R. A. van Santen, *J. Phys. Chem. B.* **2002**, 106, 9863-9872. (b) B. Qiao, A. Wang, X. Yang, L. F. Allard, Z. Jiang, Y. Cui, J. Liu, J. Li, T. Zhang. *Nat. Chem*. **2011**, 3, 634-641. (c) F. Calle-Vallejo, J. I. Martínez, J. M. García-Lastra, P. Sautet, D. Loffreda. *Angew. Chem. Int. Ed.* **2014**, 53, 8316-8319.

11 G. A. Tritsaris, J. Greeley, J. Rossmeisl, J. K. Nørskov. *Catal. Lett*. **2011**, 141, 909-913.

12 C. Rong, D. Li, V. Nandwana, N. Poudyal, Y. Ding, Z. L. Wang, H. Zeng, J. P. Liu. *Adv. Mater*. **2006**, 18, 2984-2988.

13 Y. Shao, G. Yin, Z. Wang, Y. Gao. *J. Power Sources.* **2007**, 167, 235-242.

14 B. Han, C. E. Carlton, A. Kongkanand, R. S. Kukreja, B. R. Theobald, L. Gan, R. O'Malley, P. Strasser, F. T. Wagner, Y. Shao-Horn. *Energy Environ. Sci*. **2015**, 8, 258-266.

15 (a) D. Y. Chung, S. W. Jun, G. Yoon, S. G. Kwon, D. Y. Shin, P. Seo, J. M. Yoo, H. Shin, Y. H. Chung, H. Kim, B. S. Mun, K. S. Lee, N. S. Lee, S. J. Yoo, D. H. Lim, K. Kang, Y. E. Sung, T. Hyeon. *J. Am. Chem. Soc.* **2016**, 137, 15478-15485. (b) X. X. Du, Y. He, X. X. Wang, J. N. Wang. *Energy Environ. Sci*. **2016**. 9, 2623-2632.

Insert Table of Contents artwork here